



Jansky Very Large Array Detections of CO(1–0) Emission in HI-absorption-selected Galaxies at $z \gtrsim 2$

B. Kaur¹, N. Kanekar¹, M. Rafelski^{2,3}, M. Neeleman⁴, J. X. Prochaska^{5,6}, and M. Revalski²¹ National Centre for Radio Astrophysics, Tata Institute of Fundamental Research, Pune University, Pune 411007, India; bkaur@ncra.tifr.res.in² Space Telescope Science Institute, 3700 San Martin Drive, Baltimore, MD 21218, USA³ Department of Physics & Astronomy, Johns Hopkins University, Baltimore, MD 21218, USA⁴ Max-Planck-Institut für Astronomie, Königstuhl 17, D-69117, Heidelberg, Germany⁵ Department of Astronomy & Astrophysics, UCO/Lick Observatory, University of California, Santa Cruz, 1156 High Street, Santa Cruz, CA 95064, USA⁶ Kavli Institute for the Physics and Mathematics of the Universe (Kavli IPMU), 5-1-5 Kashiwanoha, Kashiwa, 277-8583, Japan

Received 2022 May 12; revised 2022 June 16; accepted 2022 June 24; published 2022 July 13

Abstract

We report a Karl G. Jansky Very Large Array search for redshifted CO(1–0) emission from three HI-absorption-selected galaxies at $z \approx 2$, identified earlier in their CO(3–2) or CO(4–3) emission. We detect CO(1–0) emission from DLA B1228-113 at $z \approx 2.1933$ and DLA J0918+1636 at $z \approx 2.5848$; these are the first detections of CO(1–0) emission in high- z HI-selected galaxies. We obtain high molecular gas masses, $M_{\text{mol}} \approx 10^{11} \times (\alpha_{\text{CO}}/4.36) M_{\odot}$, for the two objects with CO(1–0) detections, which are a factor of ≈ 1.5 –2 lower than earlier estimates. We determine the excitation of the mid- J CO rotational levels relative to the $J = 1$ level, r_{J1} , in HI-selected galaxies for the first time, obtaining $r_{31} = 1.00 \pm 0.20$ and $r_{41} = 1.03 \pm 0.23$ for DLA J0918+1636, and $r_{31} = 0.86 \pm 0.21$ for DLA B1228-113. These values are consistent with thermal excitation of the $J = 3$ and $J = 4$ levels. The excitation of the $J = 3$ level in the HI-selected galaxies is similar to that seen in massive main-sequence and submillimeter galaxies at $z \gtrsim 2$, but higher than that in main-sequence galaxies at $z \approx 1.5$; the higher excitation of the galaxies at $z \gtrsim 2$ is likely to be due to their higher star formation rate (SFR) surface density. We use Hubble Space Telescope Wide Field Camera 3 imaging to detect the rest-frame near-ultraviolet (NUV) emission of DLA B1228-113, obtaining an NUV SFR of $4.44 \pm 0.47 M_{\odot} \text{ yr}^{-1}$, significantly lower than that obtained from the total infrared luminosity, indicating significant dust extinction in the $z \approx 2.1933$ galaxy.

Unified Astronomy Thesaurus concepts: High-redshift galaxies (734); CO line emission (262); Damped Lyman-alpha systems (349)

1. Introduction

The highest HI column density absorption systems in quasar (QSO) spectra, the damped Ly α absorbers (DLAs), arise from gas associated with high-redshift galaxies (e.g., Wolfe et al. 2005). Such absorbers provide a route to identifying high- z galaxies without the luminosity bias that afflicts galaxy samples selected directly via their emission. Understanding the nature of these HI-absorption-selected galaxies is critical for an unbiased understanding of galaxy evolution. Unfortunately, the proximity of the faint foreground galaxy to the bright background QSO has meant that, despite many studies, it has been difficult to even identify, let alone characterize, the high- z , HI-selected galaxies via optical imaging and spectroscopy (e.g., Fumagalli et al. 2015; Krogager et al. 2017).

Recently, the Atacama Large Millimeter/submillimeter Array (ALMA) has opened new windows on HI-selected galaxies via their redshifted [C II] 158 μm and CO emission. Besides the characterization of HI-selected galaxies at intermediate redshifts, $z \approx 0.6$ (e.g., Kanekar et al. 2018; Møller et al. 2018; Klitsch et al. 2019; Péroux et al. 2019), this has resulted in the identification of more than a dozen such galaxies at $z \approx 2$ (Fynbo et al. 2018; Kanekar et al. 2020; Neeleman et al. 2018) and $z \approx 4$ (Neeleman et al. 2017, 2019). Perhaps the most remarkable results from these studies are the large impact parameters to the QSO sight line of

the galaxies at $z \approx 4$ (Neeleman et al. 2017, 2019), the high molecular gas masses of the galaxies at $z \approx 2$ (Kanekar et al. 2020), and the identification of a cold, dusty, rotating disk at $z \approx 4.26$ (Neeleman et al. 2020). Multiwavelength observations are now under way to obtain a detailed understanding of these galaxies, by characterizing their stellar and gas properties, star formation activity, etc. (e.g., Prochaska et al. 2019; Kaur et al. 2021; Klitsch et al. 2022).

For the $z \approx 2$ HI-selected galaxies, the high inferred molecular gas masses, $M_{\text{mol}} \approx (1.3 - 20.7) \times 10^{10} M_{\odot}$ (Kanekar et al. 2020), were obtained from the CO(3–2) or CO(4–3) mid- J rotational transitions. These estimates are based on two critical assumptions, subthermal excitation of the CO $J = 3$ or $J = 4$ levels relative to the $J = 1$ level, and the value of the CO-to-H₂ conversion factor, α_{CO} (e.g., Tacconi et al. 2020). Direct observations of the CO(1–0) line are critical to remove the first of these assumptions, and obtain more accurate molecular gas mass estimates. Combining the CO(1–0) line luminosity with the luminosity in the higher- J CO lines also allows one to determine the CO excitation and thus probe physical conditions in the molecular gas (e.g., Carilli & Walter 2013). Indeed, studies in the local universe have shown that the CO excitation is related to the value of α_{CO} : high-excitation galaxies like ultraluminous infrared galaxies (ULIRGs) and QSO hosts have lower α_{CO} values [$\alpha_{\text{CO}} \approx 1.0 M_{\odot} (\text{K km s}^{-1} \text{ pc}^2)^{-1}$] than low-excitation objects like the Milky Way and nearby disk galaxies ($\alpha_{\text{CO}} \approx 4.3 M_{\odot} (\text{K km s}^{-1} \text{ pc}^2)^{-1}$; e.g., Bolatto et al. 2013).

At high redshifts, CO(1–0) studies have so far only been carried out in bright, emission-selected galaxies, mostly QSO



Original content from this work may be used under the terms of the [Creative Commons Attribution 4.0 licence](https://creativecommons.org/licenses/by/4.0/). Any further distribution of this work must maintain attribution to the author(s) and the title of the work, journal citation and DOI.

Table 1
JVLA Ka -band Observations and Results

DLA	z_{QSO}	z_{abs}	z_{gal}	ν_{obs} (GHz)	Beam (" × ")	RMS _{CO} ($\mu\text{Jy beam}^{-1}$)	$\int S_{\text{CO}} dV$ (Jy km s^{-1})	$L'_{\text{CO}(1-0)}$ ($10^{10} \text{ K km s}^{-1} \text{ pc}^2$)	M_{mol} ($10^{10} M_{\odot}$)
B0551-366	2.317	1.9622	1.9615	38.92	5.8×1.6	99	<0.057	<1.14	<5.0
B1228-113	3.528	2.1929	2.1933	36.10	3.1×2.0	94	0.094 ± 0.023	2.29 ± 0.56	10.0 ± 2.4
J0918+1636	3.096	2.5832	2.5848	32.15	2.8×2.3	57	0.082 ± 0.016	2.65 ± 0.51	11.5 ± 2.2

Note. The columns are (1) the galaxy name; (2) the QSO redshift; (3) the absorption redshift, z_{abs} ; (4) the galaxy redshift, z_{gal} , from the higher- J CO lines; (5) the redshifted CO(1–0) line frequency, in GHz; (6) the synthesized beam, in " × "; (7) the rms noise, in $\mu\text{Jy beam}^{-1}$, at a velocity resolution of 100 km s^{-1} ; (8) the integrated CO line flux density, in Jy km s^{-1} ; (9) the CO(1–0) line luminosity, $L'_{\text{CO}(1-0)}$; and (10) the molecular gas mass, M_{mol} , assuming $\alpha_{\text{CO}} = 4.36 M_{\odot} (\text{K km s}^{-1} \text{ pc}^2)^{-1}$. For the CO(1–0) nondetection in B0551-366, the last three columns list the 3σ upper limits on $\int S_{\text{CO}} dV$, $L'_{\text{CO}(1-0)}$, and M_{mol} , for an assumed line FWHM of 300 km s^{-1} (Kanekar et al. 2020).

hosts, submillimeter galaxies (SMGs), lensed galaxies, and massive main-sequence galaxies (e.g., Aravena et al. 2014; Bolatto et al. 2015; Sharon et al. 2016; Riechers et al. 2020). In this Letter, we report the first detections of redshifted CO(1–0) emission from HI-selected galaxies at $z \approx 2$, obtained with the Karl G. Jansky Very Large Array (JVLA).⁷ We also report Hubble Space Telescope (HST) Wide Field Camera 3 (WFC3) imaging of the rest-frame near-ultraviolet (NUV) continuum emission for one of the HI-selected galaxies, which shows that the object is a dusty galaxy.

2. Observations, Data Analysis, and Results

2.1. JVLA Observations and Data Analysis

We used the JVLA Ka -band receivers in the D-array to search for redshifted CO(1–0) emission from the HI-selected galaxies at $z \approx 1.9615$ toward QSO B0551-366, $z \approx 2.1933$ toward PKS B1228-113, and $z \approx 2.5848$ toward QSO J0918+1636 in 2019 November and December (Proposal ID: VLA/19B-271; PI: N. Kanekar). The three galaxies (hereafter DLA B0551-366, DLA B1228-113, and DLA J0918+1636) had been earlier detected with ALMA in their CO(4–3) or CO(3–2) emissions (Neeleman et al. 2018; Fynbo et al. 2018; Kanekar et al. 2020).

The JVLA observations used the WIDAR correlator in 8-bit mode, with two 1 GHz intermediate-frequency (IF) bands, one covering the redshifted CO line frequency for the target galaxy, and two polarizations. Each IF band was divided into eight 128 MHz digital subbands, with each subband further divided into 512 and 128 channels, for line and off-line subbands, respectively. This yielded a velocity coverage of $\approx 800\text{--}955 \text{ km s}^{-1}$ for the subband covering the redshifted CO line frequency, albeit with lower sensitivity at the subband edges, and a raw velocity resolution of $\approx 2 \text{ km s}^{-1}$. Observations of the targets were interleaved with runs on nearby phase calibrators every 5 minutes; in addition, a standard flux calibrator was observed once in each session. The on-source times were 2.1–5.8 hr for the three galaxies.

All data were analyzed in the Astronomical Image Processing System package (“classic” AIPS; Greisen 2003), using standard procedures. After identifying and editing out malfunctioning antennas and any data affected by systematic errors, we used the calibrator data to determine the antenna-based complex gains and bandpass shapes. The gains and bandpasses were applied to the data for each target, and the calibrated target visibilities then split out into a new data set.

For each target, the central channels of each subband of this data set were averaged together, and the resulting data sets were imaged to search for any continuum emission in each field. Although continuum emission was detected from two QSOs, only PKS B1228-113 was found to have a sufficient flux density for self-calibration. The self-calibration for PKS B1228-113 followed a standard iterative procedure, with multiple rounds of imaging and phase-only self-calibration, followed by amplitude-and-phase self-calibration and data editing, until neither the image nor the residual visibilities showed any improvement on further self-calibration. The improved complex gains for DLA B1228-113 were applied to the multichannel data to produce the final calibrated data set for this field.

Next, for each target, the task UVSUB was used to subtract out all continuum emission from the calibrated visibilities. The residual multichannel visibility data sets were then imaged in the Common Astronomy Software Applications package (CASA version 5.6; McMullin et al. 2007), using natural weighting in the barycentric frame, to produce spectral cubes at velocity resolutions of $50\text{--}100 \text{ km s}^{-1}$. The FWHM of the JVLA synthesized beams is $\approx 1''.6\text{--}5''.8$ for the three targets, larger than the size of the ALMA CO emission (Kanekar et al. 2020); we hence do not expect any of the CO(1–0) emission to be resolved out in the JVLA images. For each galaxy, a CO(1–0) emission spectrum was extracted by taking a cut through its cube at the location of the ALMA CO emission. Finally, in the case of DLA B1228-113 and DLA J0918+1636, which showed detections of CO(1–0) emission at $>4\sigma$ significance, we also made images of the CO emission, at velocity resolutions matched to the line FWHMs. The observational details and results are summarized in Table 1.

2.2. HST Observations and Data Analysis

The HST WFC3 observations of DLA B1228-113 were carried out in late 2019 (PID: 15882; PI: Kanekar), using the F105W filter to cover the rest-frame NUV stellar continuum from the $z \approx 2.1933$ galaxy. A single orbit was obtained, using a WIDE-7 dither pattern increased by a factor of 3 over the pattern described in the Instrument Science Report (ISR 2016-14; Anderson 2016), in order to obtain cleaner images by dithering over the size of the IR blobs.

The data were calibrated using the new IR filter-dependent sky flats (WFC3 ISR 2021-01; Mack et al. 2021). Image mosaics were made using AstroDrizzle (Hack et al. 2020), drizzling to a scale of $0''.06 \text{ pixel}^{-1}$. TweakReg was used to astrometrically align the image to the GAIA DR2 catalog (Gaia Collaboration et al. 2018), yielding an absolute astrometric

⁷ We assume a flat Λ cold dark matter cosmology, with $\Omega_{\Lambda} = 0.685$, $\Omega_m = 0.315$, and $H_0 = 67.4 \text{ km s}^{-1} \text{ Mpc}^{-1}$ (Planck Collaboration 2020).

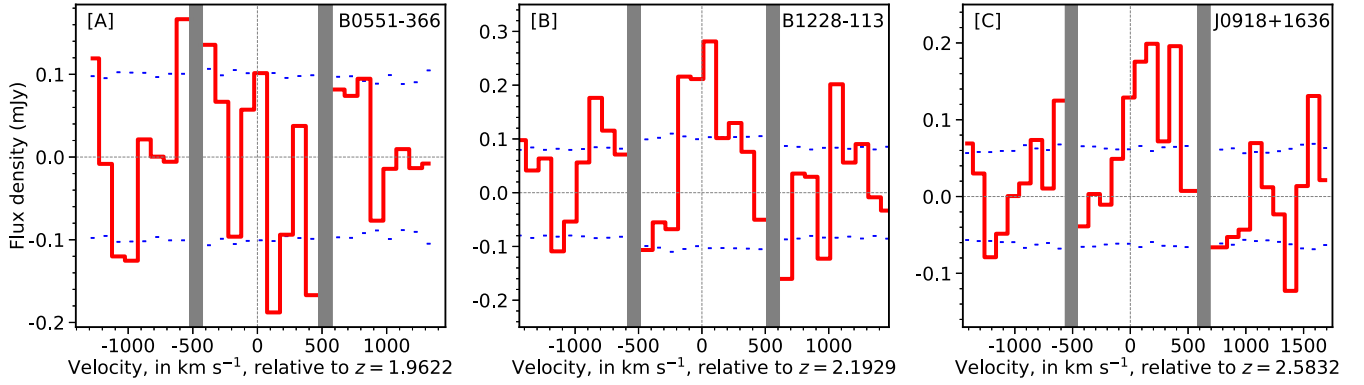


Figure 1. JVL A CO(1–0) spectra from (A) DLA B0551-366 at $z = 1.9615$, (B) DLA B1228-113 at $z = 2.1933$, and (C) DLA J0918+1636 at $z = 2.5848$. The vertical gray bands indicate the edges of the digital subbands of the WIDAR correlator, which have significantly lower sensitivity. The blue dashed curves in each panel indicate the $\pm 1\sigma$ error at each velocity channel.

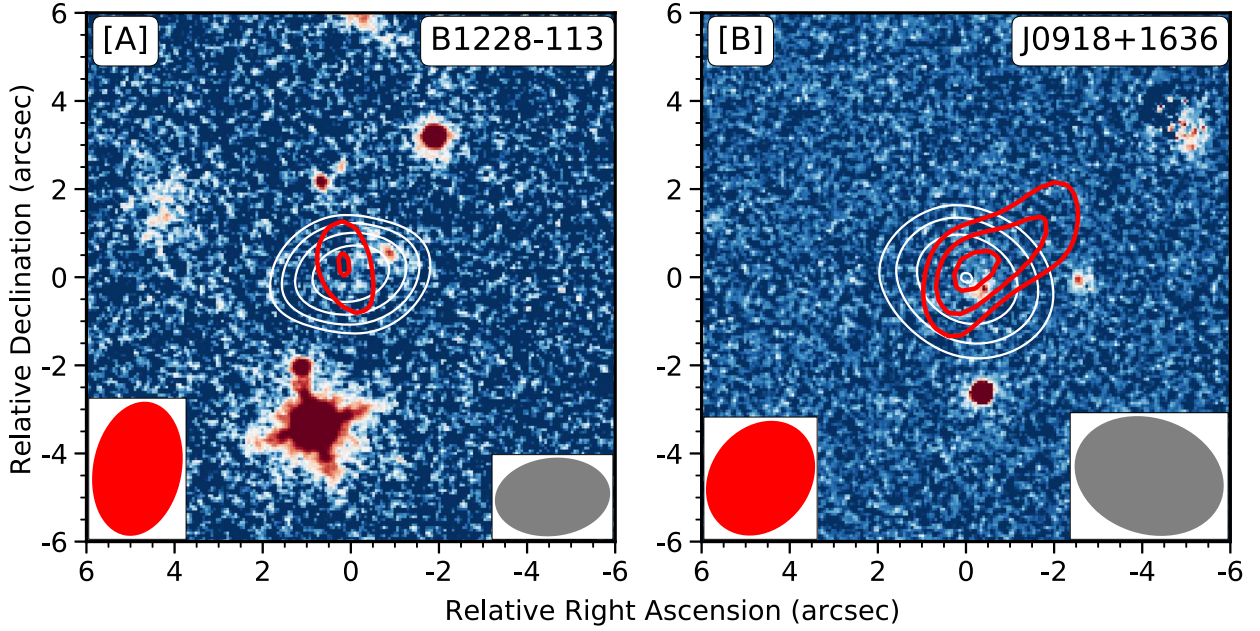


Figure 2. JVL A CO(1–0) integrated emission (red contours) overlaid on the ALMA CO(3–2) emission (white contours) and the HST WFC3 F105W image (in color) for (A) DLA B1228-113 at $z = 2.1933$ and (B) J0918+1636 at $z = 2.5848$, respectively. The left and right insets in each panel show, respectively, the JVL A (red) and ALMA (gray) synthesized beams. The CO(1–0) contours are at $(-3.0, 3.0, 4.0, 5.0) \times \sigma$ significance (note that there are no negative contours with $\geq 3\sigma$ significance), while the outermost CO(3–2) contour is at 6σ significance, with successive later contours increasing by factors of $\sqrt{2}$.

uncertainty of $\approx 0''.01$. The effective angular resolution of the HST WFC3 image is $\approx 0''.3$, based on a Gaussian fit to the point-spread function (PSF) of the quasar.

2.3. Results

Our JVL A observations yielded detections of CO(1–0) emission at $>4\sigma$ significance from the HI-selected galaxies at $z \approx 2.1933$ toward PKS B1228-113 and $z \approx 2.5848$ toward QSO J0918+1636. We also obtained an upper limit to the CO(1–0) line luminosity for the $z \approx 1.9615$ galaxy toward QSO B0551-366. Figure 1 shows the JVL A CO(1–0) spectra of the three HI-selected galaxies, while Figure 2 shows the CO(1–0) images of DLA B1228-113 and DLA J0918+1636 (in red contours), overlaid on the ALMA CO(3–2) images (in white contours), and the HST WFC3 images (in color; Fynbo et al. 2018, this work) of the two fields. For DLA B1228-113 and DLA J0918+1636, the detected CO(1–0) emission agrees in both position and velocity with the ALMA CO(3–2) emission. The

measured velocity-integrated CO(1–0) line flux densities and inferred CO line luminosities for the three galaxies are listed in Table 1. Here, the 3σ upper limits for DLA B0551-366 assume that the CO(1–0) emission has an FWHM of 300 km s^{-1} , equal to that of the CO(4–3) emission (Kanekar et al. 2020). The CO(1–0) line luminosities yield molecular gas masses of $(10.0 \pm 2.4) \times (\alpha_{\text{CO}}/4.36) \times 10^{10} M_{\odot}$ (DLA B1228-113), $(11.5 \pm 2.2) \times (\alpha_{\text{CO}}/4.36) \times 10^{10} M_{\odot}$ (DLA J0918+1636), and $< 5.0 \times (\alpha_{\text{CO}}/4.36) \times 10^{10} M_{\odot}$ (3σ limit; DLA B0551-366), where we have assumed $\alpha_{\text{CO}} = 4.36 M_{\odot} (\text{K km s}^{-1} \text{ pc}^2)^{-1}$ (Bolatto et al. 2013; Tacconi et al. 2020).

Both DLA J0918+1636 and DLA B1228-113 are detected in HST rest-frame NUV imaging. The HST images of DLA J0918+1636 are presented and described in Fynbo et al. (2018), and yield a half-light radius of $0''.30$ (J. P. U. Fynbo 2021, private communication). In the case of DLA B1228-113, the rest-frame NUV emission is detected in our HST WFC3 F105W image (see Figure 2(A)), at R.A. = $12^{\text{h}}30^{\text{m}}55^{\text{s}}.44$, decl. = $-11^{\circ}39'05''.87$, at an offset of $\approx 0''.9$ ($\approx 7.7 \text{ kpc}$) from the CO(3–2)

Table 2
The CO Excitation of the Three H I-selected Galaxies at $z \approx 2$

DLA	z_{gal}	r_{31}	r_{41}	r_{51}	r_{61}	Refs.
B0551-366	1.9615	...	>0.48	>0.24	>0.07	1,2
B1228-113	2.1933	0.86 ± 0.21	0.18 ± 0.05	1-3
J0918+1636	2.5848	1.00 ± 0.20	1.03 ± 0.23	0.39 ± 0.09	...	1,2,4

Note. The columns are (1) the galaxy name; (2) the galaxy redshift, z_{gal} ; (3) the ratio r_{31} ; (4) the ratio r_{41} ; (5) the ratio r_{51} ; (6) the ratio r_{61} ; and (7) references for the higher- J CO studies: (1) Kanekar et al. (2020); (2) Klitsch et al. (2022); (3) Neeleman et al. (2018); (4) Fynbo et al. (2018).

emission. We emphasize that no rest-frame NUV emission is detected at the center of the CO emission (see the discussion in Section 3).

We obtained photometry of DLA B1228-113 using Source Extractor v.2.19.5 (Bertin & Arnouts 1996), measuring the total flux using $\text{flux}_{\text{auto}}$, which gives the flux within an elliptical aperture with the Kron radius (Kron 1980). This yielded an AB magnitude of $m_{AB} \approx 24.72 \pm 0.12$, a half-light radius of $0''.33$, and a Kron radius of $0''.46$. To infer the star formation rate (SFR) of the galaxy, we assume that it has a Chabrier initial mass function (Chabrier 2003) and a flat spectrum in L_{ν} between rest-frame wavelengths of $\approx 3280\text{\AA}$ and 2300\AA (Kennicutt 1998). Applying the local relation between rest-frame NUV 2300\AA luminosity and SFR (Kennicutt & Evans 2012) then yields an SFR of $4.44 \pm 0.47 M_{\odot} \text{ yr}^{-1}$.

Finally, we combined the rest-frame NUV half-light radii of DLA B1228-113 ($r_{1/2} = 0''.33$) and DLA J0918+1636 ($r_{1/2} = 0''.30$) with the galaxy SFRs ($87 M_{\odot} \text{ yr}^{-1}$ and $229 M_{\odot} \text{ yr}^{-1}$, obtained from SED fits; Klitsch et al. 2022), to obtain SFR surface densities of $1.8 M_{\odot} \text{ yr}^{-1} \text{ kpc}^2$ (DLA B1228-113) and $6.2 M_{\odot} \text{ yr}^{-1} \text{ kpc}^2$ (DLA J0918+1636).

3. Discussion

3.1. Molecular Gas Masses

We have obtained the first detections of CO(1–0) emission in high-redshift H I-selected galaxies. The measured CO(1–0) line luminosities yield direct estimates of the molecular gas mass, without the need for assumptions regarding the CO excitation. We continue to obtain high molecular gas masses in DLA B1228-113 and DLA J0918+1636, albeit a factor of ≈ 1.5 lower than the estimates from the CO(3–2) line (Neeleman et al. 2018; Fynbo et al. 2018; Kanekar et al. 2020). For DLA B0551-366, we have placed an upper limit on its CO(1–0) line luminosity, and thus on its molecular gas mass, $M_{\text{mol}} < 5.0 \times (\alpha_{\text{CO}}/4.36) \times 10^{10} M_{\odot}$. This upper limit is again lower than (but, given the uncertainties, consistent with) the estimate $M_{\text{mol}} = (5.67 \pm 0.68) \times (\alpha_{\text{CO}}/4.36) \times 10^{10} M_{\odot}$, obtained by Kanekar et al. (2020) from the CO(4–3) line.

Our molecular gas masses, inferred from the CO(1–0) line, are thus systematically lower, by a factor of ≈ 1.5 , than the values obtained from the mid- J rotational lines (Kanekar et al. 2020). This indicates that the three H I-selected galaxies do not have substantial amounts of cold, low-excitation molecular gas (e.g., Papadopoulos et al. 2001). The lower gas mass estimates obtained here are because the earlier studies assumed subthermal excitation of the mid- J CO rotational levels to estimate the CO(1–0) line luminosity, and thence the molecular gas mass.

The main remaining uncertainty in the molecular gas mass estimates for our H I-selected galaxies is the value of the CO-to- H_2 conversion factor, α_{CO} . Estimates of the stellar mass

and SFR from fits to the broadband spectral energy distribution (SED; Klitsch et al. 2022) find that both DLA B1228-113 and DLA J0918+1636 lie slightly (≈ 0.5 – 0.6 dex) above the galaxy main sequence at their redshifts, but within the spread of the main sequence (e.g., Whitaker et al. 2012; Schreiber et al. 2015), especially given the large errors in the current SFR estimates. Thus, at present, there is no significant evidence that DLA B1228-113 or DLA J0918+1636 are starburst galaxies that might have $\alpha_{\text{CO}} \ll 4 M_{\odot} (\text{K km s}^{-1} \text{ pc}^2)^{-1}$ (e.g., Magdis et al. 2012). Further, the galaxy metallicities inferred from the stellar mass–metallicity relation at $z \approx 2$ are consistent with solar metallicity (Klitsch et al. 2022). We will hence assume $\alpha_{\text{CO}} \approx 4.36 M_{\odot} (\text{K km s}^{-1} \text{ pc}^2)^{-1}$ for these systems (e.g., Bolatto et al. 2013; Tacconi et al. 2020), applicable to high- z main-sequence galaxies with solar metallicity.

Combining the SFR estimates of Klitsch et al. (2022) with our molecular gas mass estimates, we obtain a molecular gas depletion timescale $\tau_{\text{dep, H}_2}$ of ≈ 1.1 Gyr (DLA B1228-113) and ≈ 0.5 Gyr (DLA J0918+1636). These are factors of ≈ 2 – 4 higher than the expected depletion times (≈ 0.25 Gyr) from the scaling relation of Tacconi et al. (2020).

3.2. The CO Spectral Line Energy Distribution in H I-selected Galaxies

Our JVLA CO(1–0) measurements allow us, for the first time, to determine the excitation of the mid- J rotational levels relative to the $J = 1$ level in H I-selected galaxies. Table 2 lists the values of $r_{J1} \equiv L'_{\text{CO}(J \rightarrow (J-1))} / L'_{\text{CO}(1-0)}$, for $J = 3$ – 6 , combining our measured CO(1–0) line luminosities with the luminosities of the higher- J lines (Kanekar et al. 2020; Klitsch et al. 2022).

Studies of high-redshift galaxies typically assume subthermal excitation of the mid- J rotational levels, with $r_{31} \approx 0.55$ and $r_{41} \approx 0.42$ (e.g., Tacconi et al. 2020). Remarkably, we find that DLA J0918+1636 has values of $r_{31} = 1.00 \pm 0.20$ and $r_{41} = 1.03 \pm 0.23$, consistent with thermal excitation of the $J = 3$ and $J = 4$ levels. We note that Klitsch et al. (2022) had earlier measured $r_{43} = 1.03$ in DLA J0918+1636, suggesting that the $J = 4$ and $J = 3$ levels are likely to show thermal excitation. Similarly, the value of $r_{31} = 0.86 \pm 0.21$ in DLA B1228-113 is consistent with thermal excitation, while the CO(1–0) nondetection in DLA B0551-366 yields the lower limit $r_{41} > 0.48$, higher than the canonical value of 0.42 (Tacconi et al. 2020). We thus find direct evidence that the mid- J rotational levels of massive H I-selected galaxies at $z \gtrsim 2$ show relatively high excitation (see also Klitsch et al. 2022).

Figure 3 plots the r_{J1} values of the three H I-selected galaxies (red symbols) against the upper rotational level quantum number, J . The dashed horizontal line at $r_{J1} = 1$ indicates thermal excitation of the rotational levels. The figure also includes data for the inner disk of the Milky Way (gray diamonds; Fixsen et al. 1999), three main-sequence (BzK)

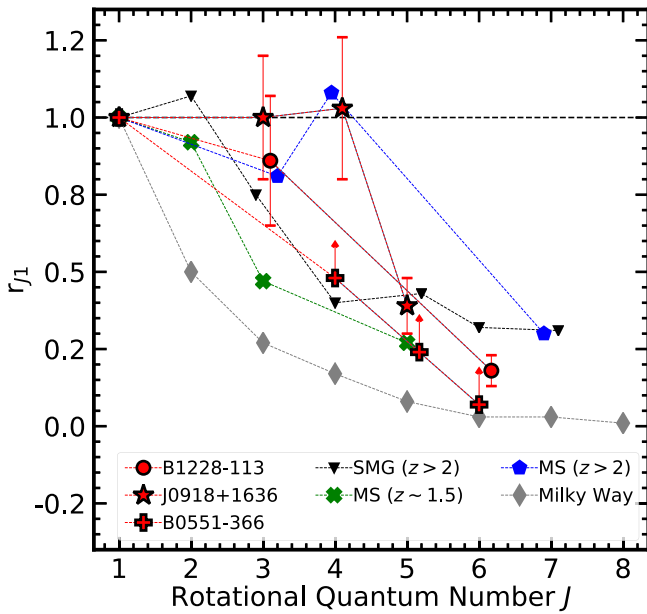


Figure 3. The ratio of the $\text{CO}(J \rightarrow J-1)$ line luminosity to the $\text{CO}(1-0)$ line luminosity, plotted as a function of the upper-state rotational quantum number, J . The dashed black line indicates the value of unity for thermal excitation. The red symbols represent the HI-selected galaxies at $z \sim 2$ (Kanekar et al. 2020; Klitsch et al. 2022, this work). For comparison, we have plotted the median value of the above ratios for main-sequence galaxies at $z \sim 1.5$ (green crosses; Daddi et al. 2015), main-sequence galaxies at $z > 2$ (blue pentagons; Riechers et al. 2010; Brisbin et al. 2019; Boogaard et al. 2020; Henríquez-Brocal et al. 2021), and submillimeter galaxies at $z > 2$ (inverted black triangles; Birkin et al. 2021). The gray diamonds indicate the CO SLED of the inner disk of the Milky Way (Fixsen et al. 1999).

galaxies at $z \approx 1.5$ (green crosses; Aravena et al. 2014; Daddi et al. 2015), five main-sequence galaxies at $z > 2$ (blue pentagons; Riechers et al. 2010; Bolatto et al. 2015; Brisbin et al. 2019; Boogaard et al. 2020; Riechers et al. 2020; Henríquez-Brocal et al. 2021), and a large sample of SMGs at $z > 2$ (inverted black triangles; Birkin et al. 2021). For the high- z main-sequence galaxies and SMGs, the figure shows the median values of r_{J1} of objects with measurements of both the $\text{CO}(1-0)$ line and higher- J CO lines. In the case of the SMGs, we have used the median CO spectral line energy distribution (SLED) of the large SMG sample of Birkin et al. (2021), who assumed $r_{21} = 0.9$ due to the paucity of $\text{CO}(1-0)$ measurements in their sample. We bypass this assumption by normalizing their r_{J1} values to $r_{31} = 0.75$, the median measured r_{31} value obtained for 18 SMGs at $z \approx 2.2-3.1$ (Sharon et al. 2016; Calistro Rivera et al. 2018).

Figure 3 shows that the three HI-selected galaxies have CO SLEDs consistent with those of massive main-sequence galaxies at $z > 2$. The excitation of the mid- J rotational levels of the HI-selected galaxies is clearly higher than that of both the inner disk of the Milky Way and main-sequence galaxies at $z \approx 1.5$. Further, the roughly thermal excitation of the $J = 3$ and $J = 4$ levels in DLA J0918+1636 (and of the $J = 3$ level in DLA B1228-113) is consistent with the excitation of the same levels in the main-sequence galaxy BX610 (Bolatto et al. 2015; Brisbin et al. 2019). It is interesting that the excitation in DLA J0918+1636 drops sharply in the $J = 5$ rotational level, with $r_{51} \approx 0.39$, well below thermal.

Figure 4(A) plots r_{31} versus redshift for DLA B1228-113, DLA J0918+1636, and the above samples of SMGs at $z > 2$,

and main-sequence galaxies at $z \approx 1.5$ and $z > 2$. Here, the individual r_{31} values are plotted for the main-sequence galaxies (e.g., Riechers et al. 2010; Daddi et al. 2015; Bolatto et al. 2015; Brisbin et al. 2019; Henríquez-Brocal et al. 2021; Boogaard et al. 2020) and the median value for the SMGs (Sharon et al. 2016). Interestingly, we find evidence that all galaxies at $z > 2$ show higher excitation of the $J = 3$ level than main-sequence galaxies at $z \approx 1.5$, by a factor of $\approx 1.5-2$. This is consistent with the result from the ALMA Spectroscopic Survey in the Hubble Ultra Deep Field (ASPECS), that galaxies at $z \geq 2$ have an intrinsically higher CO excitation than those at $z < 2$ (Boogaard et al. 2020). As noted by the latter authors, the likely cause of the higher CO excitation is the higher SFR surface density Σ_{SFR} in higher- z galaxies (e.g., Shibuya et al. 2015); simulations have found that the CO excitation is closely linked to the SFR surface density, with a higher excitation obtained for higher values of Σ_{SFR} (Narayanan & Krumholz 2014; Bournaud et al. 2015). Figure 4(B) plots r_{31} versus SFR surface density⁸ for our HI-selected galaxies and the main-sequence galaxies⁸ of the left panel. It is clear that the SFR surface densities of the HI-selected galaxies and the $z > 2$ main-sequence galaxies are higher by factors of $\approx 2-10$ than those of the main-sequence galaxies at $z \approx 1.5$, consistent with the higher CO excitation of the higher- z sample.

3.3. Stellar Properties of DLA B1228-113

Finally, our SFR estimate of $4.44 \pm 0.47 M_{\odot} \text{ yr}^{-1}$ for the $z \approx 2.1933$ HI-selected galaxy DLA B1228-113 from its rest-frame NUV continuum is consistent with the estimate of $\approx 3.9 M_{\odot} \text{ yr}^{-1}$ from the $\text{H}\alpha$ line (Neeleman et al. 2018). The total SFR, estimated from both the total infrared luminosity and fits to the broadband SED, is far higher than the above estimates, $\approx (87-100) M_{\odot} \text{ yr}^{-1}$ (Neeleman et al. 2018; Klitsch et al. 2022), implying a high dust extinction. Figure 2(A) shows that the rest-frame NUV emission detected in the HST WFC3 image is offset from the peak of the ALMA $\text{CO}(3-2)$ emission, by ≈ 8 kpc. Combined with the very large $\text{CO}(3-2)$ line FWHM ($\approx 600 \text{ km s}^{-1}$; Neeleman et al. 2018), this suggests that the CO emission may arise from two merging galaxies, one of which has a high extinction and is hence not visible in the HST WFC3 image. High angular resolution CO mapping studies would be of much interest to directly probe this issue. Finally, we cannot formally rule out the possibility that the detected NUV emission arises from an interloper at a different redshift; if so, this would imply an even higher dust extinction for the $z \approx 2.1933$ HI-selected galaxy.

4. Summary

We report JVLA detections of $\text{CO}(1-0)$ emission in two HI-selected galaxies at $z \approx 2.1933$ and $z \approx 2.5848$, and an upper limit to the $\text{CO}(1-0)$ line luminosity in a third HI-selected galaxy at $z \approx 1.9615$. These are the first detections of $\text{CO}(1-0)$ emission in HI-selected galaxies at high redshifts, $z \gtrsim 2$, allowing us to directly estimate the molecular gas mass of the galaxies without assumptions about their CO excitation. We obtain molecular gas masses $\approx 1.5-2$ times lower than earlier estimates based on the mid- J CO lines. We find thermal excitation of the $J = 3$ and $J = 4$ rotational levels in the $z = 2.5848$ galaxy DLA J0918+1636, and near-thermal

⁸ The Σ_{SFR} values for the main-sequence galaxies are from Tacconi et al. (2013) and Boogaard et al. (2020).

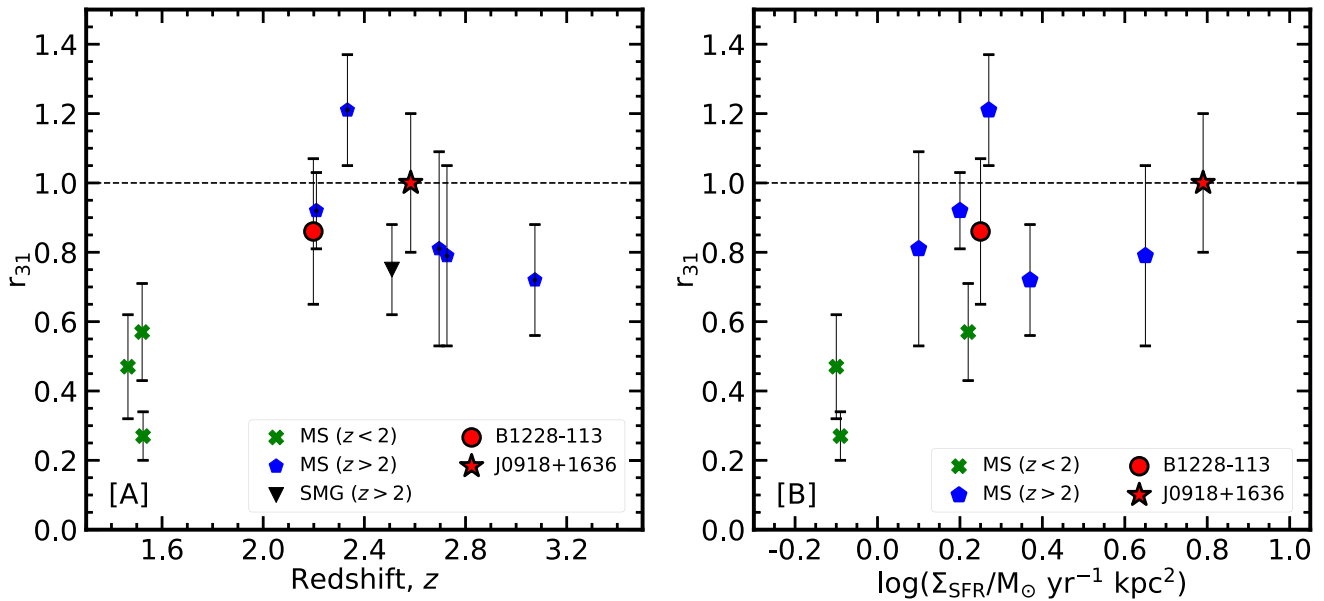


Figure 4. The ratio of the CO(3–2) line luminosity to the CO(1–0) line luminosity (r_{31}), plotted as a function of (A) redshift and (B) SFR surface density, for the H I-selected galaxies of this work (red symbols), BzK galaxies at $z \approx 1.5$ (green crosses; Daddi et al. 2015), and main-sequence galaxies at $z > 2$ (blue pentagons; Riechers et al. 2010; Brisbin et al. 2019; Boogaard et al. 2020; Henríquez-Brocal et al. 2021). The left panel also shows the median r_{31} value for submillimeter galaxies at $z > 2$ (inverted black triangles; Sharon et al. 2016). The dashed horizontal line in both panels indicates $r_{31} = 1$, for thermal excitation.

excitation of the $J=3$ level in the $z = 2.1933$ galaxy DLA B1228-113. In both cases, the CO excitation of the mid- J rotational levels is higher than that typically assumed for main-sequence galaxies at $z \approx 2$. We also find evidence for higher excitation of the $J=3$ level in H I-selected galaxies, main-sequence galaxies, and SMGs at $z \gtrsim 2$ than in main-sequence galaxies at $z \approx 1.5$. This appears to arise due to a higher SFR surface density in the former types of galaxies. Finally, we used HST WFC3 imaging to detect rest-frame NUV emission from the $z \approx 2.1933$ galaxy DLA B1228-113, obtaining an NUV SFR of $4.44 \pm 0.47 M_{\odot} \text{ yr}^{-1}$. This is a factor of ≈ 20 lower than the SFR estimated from the total infrared luminosity or from SED fitting, confirming that the object is a highly dusty galaxy. The stellar NUV emission appears slightly offset from the ALMA CO(3–2) emission, suggesting that the CO and NUV emission may arise from a pair of merging galaxies, one of which is highly obscured and hence not detected in its stellar emission.

We thank Johan Fynbo for providing us with the HST fit results for DLA J0918+1636. B.K. and N.K. acknowledge the Department of Atomic Energy for funding support, under project 12-R&D-TFR-5.02-0700. M.N. acknowledges support from ERC advanced grant 740246 (Cosmic_Gas). This research is based on observations made with the NASA/ESA Hubble Space Telescope obtained from the Space Telescope Science Institute, which is operated by the Association of Universities for Research in Astronomy, Inc., under NASA contract NAS 5-26555. Support for Program number 15882 was provided through a grant from the STScI under NASA contract NAS5-26555. The National Radio Astronomy Observatory is a facility of the National Science Foundation operated under cooperative agreement by Associated Universities, Inc. This material is based upon work supported by the National Science Foundation under grant No. 2107989.

Software: DrizzlePac (Hack et al. 2020), CASA (v5.6; McMullin et al. 2007), AIPS (Greisen 2003), ASTROPY (Astropy Collaboration et al. 2013).

ORCID iDs

B. Kaur <https://orcid.org/0000-0002-1372-0686>
 N. Kanekar <https://orcid.org/0000-0002-9757-7206>
 M. Rafelski <https://orcid.org/0000-0002-9946-4731>
 M. Neeleman <https://orcid.org/0000-0002-9838-8191>
 J. X. Prochaska <https://orcid.org/0000-0002-7738-6875>
 M. Revalski <https://orcid.org/0000-0002-4917-7873>

References

- Anderson, J. 2016, Supplemental Dither Patterns for WFC3/IR, Space Telescope WFC Instrument Science Report
- Aravena, M., Hodge, J. A., Wagg, J., et al. 2014, *MNRAS*, 442, 558
- Astropy Collaboration, Robitaille, T. P., Tollerud, E. J., et al. 2013, *A&A*, 558, A33
- Bertin, E., & Arnouts, S. 1996, *A&AS*, 117, 393
- Birkin, J. E., Weiss, A., Wardlow, J. L., et al. 2021, *MNRAS*, 501, 3926
- Bolatto, A. D., Wolfire, M., & Leroy, A. K. 2013, *ARA&A*, 51, 207
- Bolatto, A. D., Warren, S. R., Leroy, A. K., et al. 2015, *ApJ*, 809, 175
- Boogaard, L. A., van der Werf, P., Weiss, A., et al. 2020, *ApJ*, 902, 109
- Bournaud, F., Daddi, E., Weiß, A., et al. 2015, *A&A*, 575, A56
- Brisbin, D., Aravena, M., Daddi, E., et al. 2019, *A&A*, 628, A104
- Calistro Rivera, G., Hodge, J. A., Smail, I., et al. 2018, *ApJ*, 863, 56
- Carilli, C. L., & Walter, F. 2013, *ARA&A*, 51, 105
- Chabrier, G. 2003, *ApJL*, 586, L133
- Daddi, E., Dannerbauer, H., Liu, D., et al. 2015, *A&A*, 577, A46
- Fixsen, D. J., Bennett, C. L., & Mather, J. C. 1999, *ApJ*, 526, 207
- Fumagalli, M., O’Meara, J. M., Prochaska, J. X., Rafelski, M., & Kanekar, N. 2015, *MNRAS*, 446, 3178
- Fynbo, J. P. U., Heintz, K. E., Neeleman, M., et al. 2018, *MNRAS*, 479, 2126
- Gaia Collaboration, Brown, A. G. A., Vallenari, A., et al. 2018, *A&A*, 616, A1
- Greisen, E. W. 2003, in *Astrophysics and Space Science Library*, Vol. 285, Information Handling in Astronomy—Historical Vistas, ed. A. Heck (Dordrecht: Kluwer), 109
- Hack, W. J., Cara, M., Sosey, M., et al. 2020, spacetelescope/drizzlepac: DrizzlepacShow affiliations, Zenodo doi:10.5281/zenodo.3743274

- Henríquez-Brocal, K., Herrera-Camus, R., Tacconi, L., et al. 2022, *A&A*, **657**, L15
- Kanekar, N., Prochaska, J., Neeleman, M., et al. 2020, *ApJL*, **901**, L5
- Kanekar, N., Prochaska, J. X., Christensen, L., et al. 2018, *ApJL*, **856**, L23
- Kaur, B., Kanekar, N., Rafelski, M., et al. 2021, *ApJ*, **921**, 68
- Kennicutt, R. C. J. 1998, *ARA&A*, **36**, 189
- Kennicutt, R. C., & Evans, N. J. 2012, *ARA&A*, **50**, 531
- Klitsch, A., Zwaan, M. A., Péroux, C., et al. 2019, *MNRAS*, **482**, L65
- Klitsch, A., Christensen, L., Valentino, F., et al. 2022, *MNRAS*, **514**, 2346
- Krogager, J. K., Møller, P., Fynbo, J. P. U., & Noterdaeme, P. 2017, *MNRAS*, **469**, 2959
- Kron, R. G. 1980, *ApJS*, **43**, 305
- Mack, J., Olszewski, H., & Pirzkal, N. 2021, WFC3/IR Filter-Dependent Sky Flats, Space Telescope WFC Instrument Science Report
- Magdis, G. E., Daddi, E., Béthermin, M., et al. 2012, *ApJ*, **760**, 6
- McMullin, J. P., Waters, B., Schiebel, D., Young, W., & Golap, K. 2007, in ASP Conf. Ser., 376, *Astronomical Data Analysis Software and Systems XVI*, ed. R. A. Shaw, F. Hill, & D. J. Bell (San Francisco, CA: ASP), 127
- Møller, P., Christensen, L., Zwaan, M. A., et al. 2018, *MNRAS*, **474**, 4039
- Narayanan, D., & Krumholz, M. R. 2014, *MNRAS*, **442**, 1411
- Neeleman, M., Kanekar, N., Prochaska, J. X., et al. 2018, *ApJL*, **856**, L12
- Neeleman, M., Kanekar, N., Prochaska, J. X., et al. 2017, *Sci*, **355**, 1285
- Neeleman, M., Kanekar, N., Prochaska, J. X., Rafelski, M. A., & Carilli, C. L. 2019, *ApJL*, **870**, L19
- Neeleman, M., Prochaska, J. X., Nissim, K., & Rafelski, M. 2020, *Natur*, **581**, 269
- Papadopoulos, P., Ivison, R., Carilli, C., & Lewis, G. 2001, *Natur*, **409**, 58
- Péroux, C., Zwaan, M. A., Klitsch, A., et al. 2019, *MNRAS*, **485**, 1595
- Planck Collaboration 2020, *A&A*, **641**, A6
- Prochaska, J. X., Neeleman, M., Kanekar, N., & Rafelski, M. 2019, *ApJL*, **886**, L35
- Riechers, D. A., Carilli, C. L., Walter, F., & Momjian, E. 2010, *ApJL*, **724**, L153
- Riechers, D. A., Boogaard, L. A., Decarli, R., et al. 2020, *ApJL*, **896**, L21
- Schreiber, C., Pannella, M., Elbaz, D., et al. 2015, *A&A*, **575**, A74
- Sharon, C. E., Riechers, D. A., Hodge, J., et al. 2016, *ApJ*, **827**, 18
- Shibuya, T., Ouchi, M., & Harikane, Y. 2015, *ApJS*, **219**, 15
- Tacconi, L. J., Genzel, R., & Sternberg, A. 2020, *ARA&A*, **58**, 157
- Tacconi, L. J., Neri, R., Genzel, R., et al. 2013, *ApJ*, **768**, 74
- Whitaker, K. E., van Dokkum, P. G., Brammer, G., & Franx, M. 2012, *ApJL*, **754**, L29
- Wolfe, A. M., Gawiser, E., & Prochaska, J. X. 2005, *ARA&A*, **43**, 861